Electronic Supplementary Material (ESI) for ChemComm.

Electronic Supplementary Information

Strong antiferromagnetic exchange between manganese phthalocyanine and ferromagnetic europium oxide

Christian Wäckerlin, Fabio Donati, Aparajita Singha, Romana Baltic, Anne-Christine Uldry, Bernard Delley, Stefano Rusponi, and Jan Dreiser

Contents

Sample preparation

The HOPG substrate was cleaved in air, immediately introduced into the vacuum system's load lock and annealed for several hours up to 800°C in ultra-high vacuum. After thorough degassing, Eu was evaporated for 30 minutes at a rate of ~3 monolayers (ML) per minute at the sample position in the presence of an O_2 partial pressure of 6×10^{-9} mbar while holding the substrate at a temperature of 550°C,[1] leading to the formation of a few nanometer thick film as confirmed from $T_c > 50$ K (Figure S4).[2] MnPc (Sigma-Aldrich) was thoroughly degassed and a submonolayer was deposited onto the freshly prepared EuO film at room temperature (deposition time: 120 s, sublimation rate: ~0.25 ML/min). The incident rates of Eu and MnPc were determined using a quartz crystal microbalance.

In order to estimate the amount of deposited molecules, the x-ray spectra of MnPc/Co shown in ref. 3 were used as a reference. Comparing the Mn L_3 peak areas normalized to the pre-edge backgrounds as well as comparing the x-ray attenuation lengths of EuO (209 nm) and Co (386 nm) at 640 eV, and considering a possible contribution of the HOPG substrate to the pre-edge background, we conclude that the coverage with molecules is less than 1.05 ML.

X-ray absorption spectroscopy

The spectra were recorded in total electron yield mode using circularly (σ^+, σ^-) and linearly polarized (σ^h, σ^v) x-rays at the X-Treme beam line at the Swiss Light Source.[4] A defocused x-ray beam was used resulting in a spot size of ~0.3×1.2 mm^2 on the sample. The XAS spectra were obtained from the sum of the spectra taken for the two circular ($\sigma^+ + \sigma^-$) or linear polarizations ($\sigma^h + \sigma^v$), respectively, and the XMCD and XNLD spectra were calculated from the differences, ($\sigma^+ - \sigma^-$) and ($\sigma^h - \sigma^v$). In order to apply the sum rules and in order to compare with calculated spectra, a polynomial and a step function were subtracted as the background. Remanent spectra were taken after magnetizing the sample in a field of 1 T. Magnetization curves $M(H)$ were taken by measuring the XAS at the edge and the pre-edge in an alternating fashion while continuously sweeping the magnetic field. This magnetic field sweep was performed for the two circular polarizations at a rate of 1 T/min.

Atomic force microscopy

The images were recorded in a commercial instrument (Digital Instruments, Dimension 3100) in air and at room temperature using tapping mode with a NSC15/AL BS cantilever from µMash.

Spin-Hamiltonian calculations

Spin Hamiltonian calculations were based on full diagonalization of the Hamiltonian described in the main text using a home-written MATLAB® code. The measured Eu magnetization was introduced in the calculations as an effective exchange field $H_{\mathrm{ex}} = k_{\mathrm{ex}} M_{\mathrm{Eu}}$. The coupling parameter k_{ex} was obtained from least-squares fits to the experimental data.

Multiplet calculations

The MultiX software[5] was used to calculate x-ray spectra for different oxidation states of the Mn ion (I, II, III). The phthalocyanine ligand as well as the EuO surface was taken into account by an effective point-charge ligand field described by the parameters *a* (axial distortion), *b* (effective charges presented by the closest N ligands), and *c* (effective axial charge below the Mn ion taking into account the effect of the surface) given in Table S1. The calculated spectra were corrected by a constant energy offset, and the values of the spin-orbit coupling and coulomb interactions for Mn (Eu) were scaled to 97% (93%) and 80% of their computed values, respectively. Line broadening was modeled by convolution with a Lorentzian of width 0.2 eV. Least-squares fits were performed with freely varying parameters *a*,*b*,*c* in order to reproduce the full set of polarization dependent Mn x-ray spectra shown in Figure 2b-d of the main text. Best-fit spectra for Mn(I), Mn(II) and Mn(III) oxidation states are plotted in Figure S1. The spectra were obtained by running separate least-squares fits for each of the above mentioned oxidation states. The fits reveal that the data are best described by Mn(II) in a high-spin (S = 5/2, L = 0) ground state, with the best-fit parameter values given in Table S1.

After fixing the oxidation state to Mn(II), additional calculations were performed starting out from the best fit ligand field in order to understand the influence of different ligand field components. The resulting spectra are presented in Figure S2. The removal of the axial charge (spectra labeled by iii) leads to a strong modification of the electronic configuration (intermediate spin, $S = 3/2$; $L = 1$). In spectra (iv) the square planar charges have been rescaled

(tetragonal distortion a = 0, axial charge c = 0, square planar charges b = -1.5) in order to re-establish the high spin state (iv). The calculated spectra (i, ii, iv) have high spin (S = 5/2, L = 0) ground states and they are qualitatively similar to the experimental data. We note that neither the removal of the tetragonal distortion (ii) nor the removal of both the axial charge and the tetragonal distortion (iv) results in a significantly larger XLD signal compared to the best fit (i). Therefore presence of a significant disordered fraction of molecules in combination with an alternative crystal field is excluded.

The calculated expectation values $\langle S_z \rangle$, $\langle L_z \rangle$ of Eu and of Mn using the best-fit parameter values given in Table S1 are reported in Table S2 and Table S3, respectively, together with the obtained correction factors c relating the true spin $\langle S_z \rangle$ and the effective spin found from the spin sum rule $\langle S_{\mathrm{eff},z} \rangle$.

Table S1 Effective point charge ligand field acting on the Mn ion placed at the origin. The parameterization used in the fits (free parameters a,b,c) is given along with the set of best-fit values. The z-axis was taken to be normal to the EuO plane and antiparallel to the x-ray beam propagation direction and to the applied magnetic field.

x (Å)	y (Å)	z (Å)	charge (e)
-2	0	a = 0.4	b = -2.53
2	0	a = 0.4	b = -2.53
0	-2	a = 0.4	b = -2.53
0	2	a = 0.4	b = -2.53
0	0	-2	c = -2.46

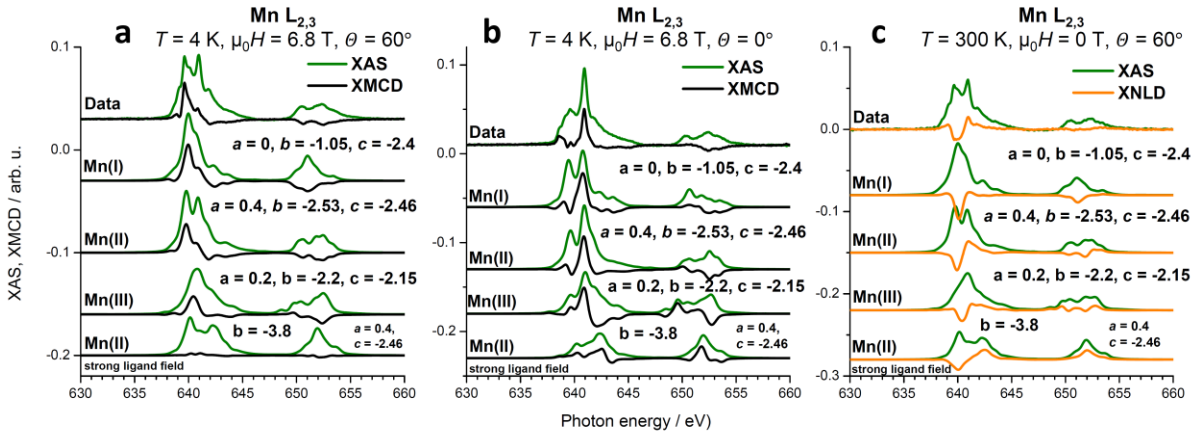

Figure S1 Comparison of the experimental Mn $L_{2,3}$ XAS/XMCD (a-b) and XNLD (c) with calculated best-fit spectra for Mn(I), Mn(II) and Mn(III) oxidation states. The spectra for Mn(I), Mn(II) and Mn(III) are obtained for $3d^6$, $3d^5$ and $3d^4$ electronic configurations of the Mn ion, respectively. The Mn(II) spectra are identical to those shown in Figure 2 of the main text. A Mn(II) intermediate spin (S = 3/2; L = 1) state, labeled as "strong ligand field" is obtained when the magnitude of the four in-plane charges in Table S1 (parameter b) is scaled up by a factor of 1.5. Details of the calculations are given in the text (ESI) and the parameters a, b and c are defined in Table S1.

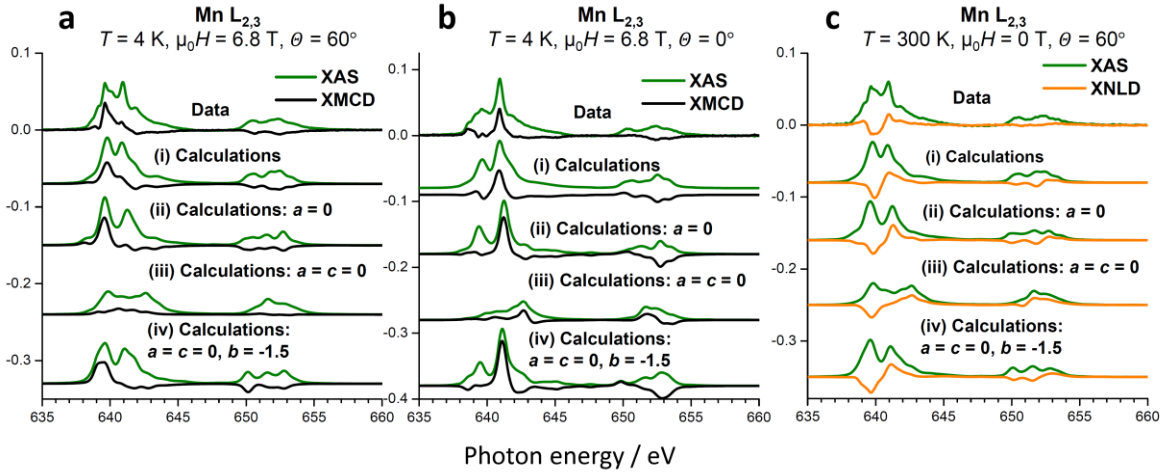

Figure S2 Comparison of the experimental Mn $L_{2,3}$ XAS/XMCD (a-b) and XNLD (c) with calculated spectra for Mn(II) using high-symmetry ligand fields described by the indicated parameter values a,b,c. The spectra labeled as (i) were obtained using the parameter values given in Table S1 for Mn(II), and they are identical to those shown in Figure 2 of the main text.

Table S2 Expectation values of the Mn $\langle S_z \rangle$, $\langle L_z \rangle$ and $\langle S_{\mathrm{eff},z} \rangle$ operators extracted from the calculated x-ray spectra at $\mu_0 H$ = 6.8 T. Here, the *z*-axis is antiparallel to the x-ray beam propagation direction and to the magnetic field. The correction factor is virtually independent of the X-ray incidence angle Θ and that it agrees very well with the values found for high-spin $3d^5$ Fe(III)[6] and Mn(II).[7]

	Ground state of multiplet		Result of sum rules when applied to the calculated spectra		Correction factor
	$\langle S_z \rangle$	$\langle L_z \rangle$	$2\langle S_{\mathrm{eff},z} \rangle$	$\langle L_z \rangle$	$c = \langle S_{\mathrm{eff},z} \rangle / \langle S_z \rangle$
Θ=0°	4.996/2	0.001	3.49	0.001	0.698
Θ=60°	4.972/2	0.002	3.36	0.001	0.677

Table S3 Expectation values of the Eu $\langle S_z \rangle$, $\langle L_z \rangle$ and $\langle S_{\mathrm{eff},z} \rangle$ operators extracted from the calculated x-ray spectra at $\mu_0 H$ = 6.8 T.

	Ground state of multiplet		Result of sum rules when applied to the calculated spectra		Correction factor
	$\langle S_z \rangle$	$\langle L_z \rangle$	$2\langle S_{\mathrm{eff},z} \rangle$	$\langle L_z \rangle$	$c = \langle S_{\mathrm{eff},z} \rangle / \langle S_z \rangle$
Θ=0°	6.926/2	0.037	6.662	0.026	0.961
Θ=60°	6.686/2	0.038	6.249	0.022	0.934

Sum rule analysis

To obtain the spin and orbital magnetic moments, the sum rules[7–9] were applied taking into account a number of holes n_h = 5 for Mn(II) consistent with the results of the MultiX calculations. From the integrated XAS and XMCD the effective spin and angular momenta shown in Table S4 are determined. For Eu(II), a number of holes n_h = 7 was used in agreement with its $4f^7$ configuration.

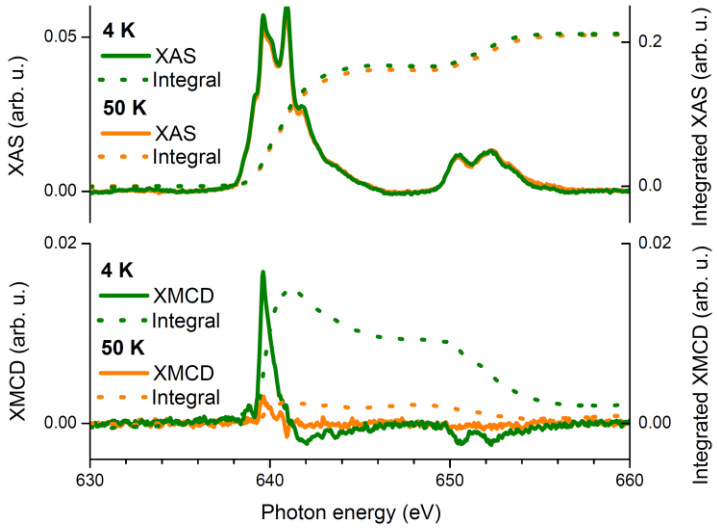

Figure S3 Example background subtracted x-ray spectra recorded at the Mn $L_{2,3}$ edges in remanence along with the corresponding integrals relevant for the sum rule analysis.

Table S4 Values of the spin and orbital magnetic moments obtained from sum-rule analyses of the Eu and Mn x-ray spectra in units of μ_B.

	EuO substrate **Eu $M_{4,5}$**			**adsorbed MnPc** **Mn $L_{2,3}$**		
$\mu_0 H$; T; Θ	$2\langle S_{eff}\rangle$	$2\langle S_z\rangle$	$\langle L_z\rangle$	$2\langle S_{eff}\rangle$	$2\langle S_z\rangle$	$\langle L_z\rangle$
6.8 T; 4 K; 0°	4.7 ± 0.3	4.9± 0.3	-0.9 ± 0.2	-2.0 ± 0.2	-2.9 ± 0.3	-0.2 ± 0.1
6.8 T; 4 K; 60°	5.4 ± 0.3	5.8 ± 0.3	-1.1 ± 0.2	-2.5 ± 0.2	-3.7 ± 0.3	-0.3 ± 0.1
0 T; 4 K; 60°	1.5 ± 0.2	1.6 ± 0.2	-0.2 ± 0.1	-1.0 ± 0.05	-1.5 ± 0.1	-0.05 ± 0.1
0 T; 50 K; 60°	0.5 ± 0.1	0.55 ± 0.1	-0.1 ± 0.05	-0.2 ± 0.05	-0.3 ± 0.1	0.0 ± 0.05
0 T; 110 K; 60°	0.0± 0.05	0.0± 0.05	0.0± 0.05	0.0± 0.03	0.0± 0.03	0.0± 0.03

High-temperature and Eu(III) x-ray spectra

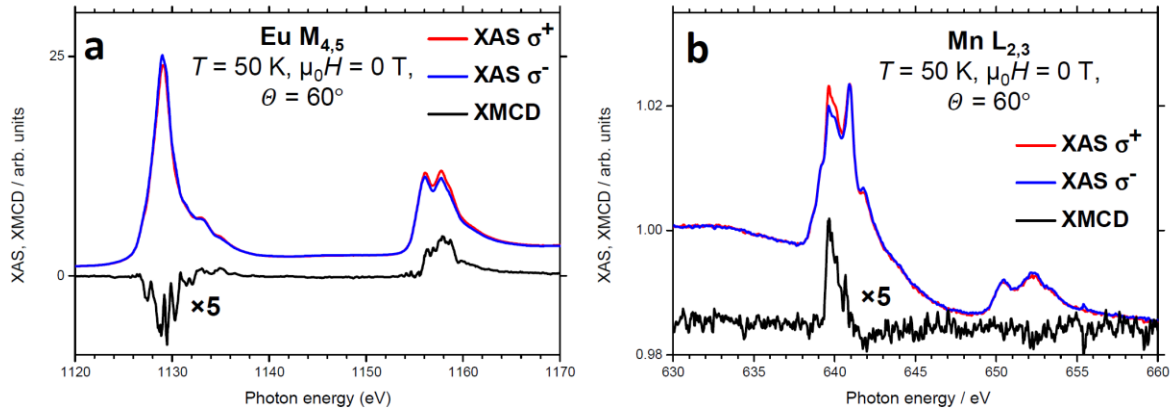

Figure S4 XAS and XMCD recorded at the Eu $M_{4,5}$ (a) and Mn $L_{2,3}$ (b) edges in remanence at T = 50 K. The Mn XMCD is shown with an offset.

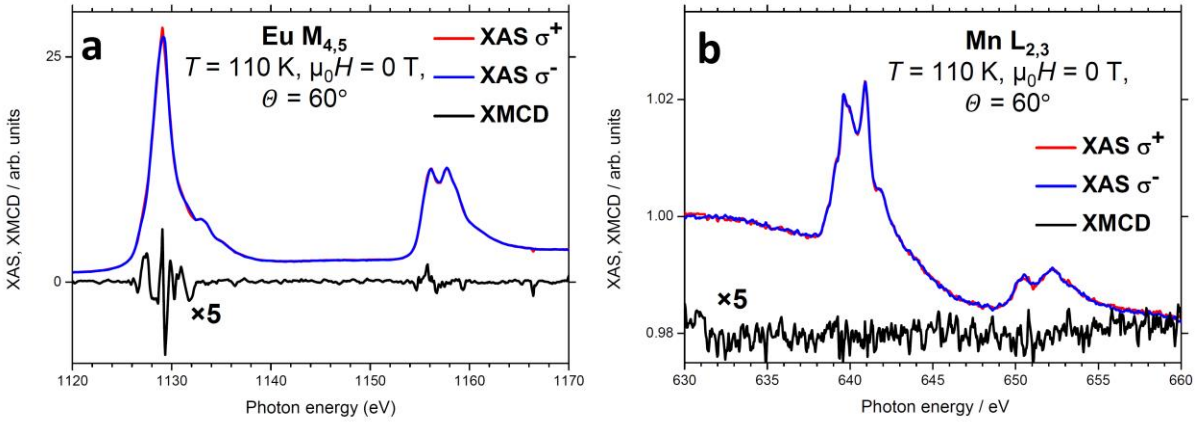

Figure S5 XAS and XMCD recorded at the Eu $M_{4,5}$ (a) and Mn $L_{2,3}$ (b) edges at $\mu_0 H$ = 0 T and T = 110 K, which is above the Curie temperature of EuO. The Mn XMCD is shown with an offset. The magnetic moments of both Eu and Mn are zero within the noise. Figures S4 and 1 reveal the presence of a remanent magnetization in Eu at 50 K and 4 K. Therefore the absence of a remanent magnetization at 110 K is inconsistent with a paramagnetic state in which the magnetization and XMCD would be inversely proportional to the temperature.

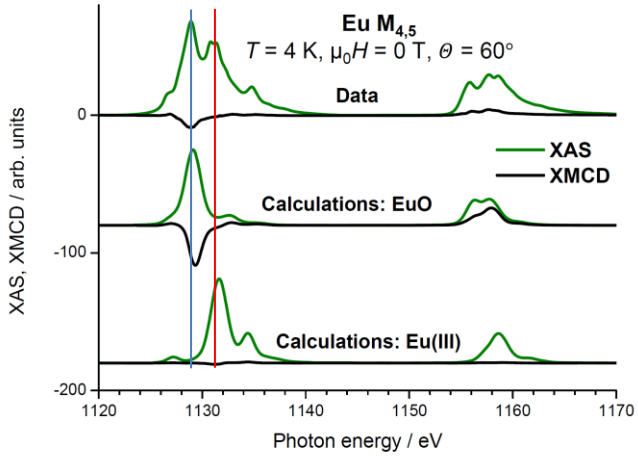

Figure S6 XAS and XMCD recorded on EuO_{1+x} at the Eu $M_{4,5}$ edges at $\mu_0 H = 0$ T and $T = 4$ K and calculated spectra. The EuO_{1+x} thin film containing a mixture of Eu(II) and Eu(III) was prepared at a similar oxygen pressure but ~1.5 times lower Eu flux. Comparison with the calculated x-ray spectra and with ref. [10], as well as the position of the feature in XMCD reveal that the XAS peak at 1129 eV corresponds to Eu(II), and the peaks at 1131 eV and 1135 eV correspond to Eu(III). A shift was applied to match the calculated Eu(II) spectra with the experimental ones. The Eu(III) spectra was shifted to match the experimental Eu_2O_3 spectra published in ref. [10].

Brillouin function model of the exchange interaction

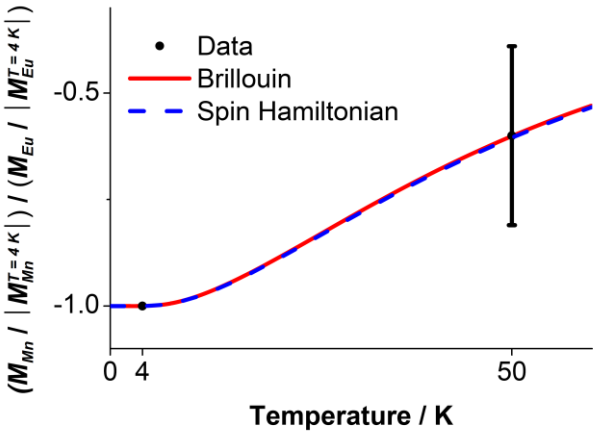

Figure S7 Estimation of the exchange energy from the normalized Mn and Eu magnetic moments at T = 4 K and T = 50 K (Table S4) using a Brillouin function model.[11–13] The normalized magnetization $M_r = M/|M_{T=4\,\mathrm{K}}|$ of Eu and Mn are described by $M_r^{\mathrm{Mn}} = M_r^{\mathrm{Eu}}\, B_J(\frac{E_{\mathrm{ex}}^B}{2k_B\,T})$, with $B_J(x) = \frac{2J+1}{2J}\coth\left(\frac{2J+1}{2J}x\right) - \frac{1}{2J}\coth\left(\frac{1}{2J}x\right)$ and $J = S_{\mathrm{Mn}} = 5/2$. The exchange energy is numerically determined to be $E_{\mathrm{ex}}^{\mathrm{B}} = -14 \pm 7$ meV, with the error obtained from the experimental uncertainties of the sum rule results. The figure displays $M_r^{\mathrm{Mn}}/M_r^{\mathrm{Eu}}$ and the corresponding Brillouin function $B_J(\frac{E_{\mathrm{ex}}^B}{2k_B\,T})$. Note that the Spin Hamiltonian calculations yield the same temperature dependence of the magnetization as the Brillouin function model.

References

1 A. G. Swartz, P. M. Odenthal, Y. Hao, R. S. Ruoff and R. K. Kawakami, *ACS Nano*, 2012, **6**, 10063–10069.

2 E. Arenholz, A. Schmehl, D. G. Schlom and G. van der Laan, *J. Appl. Phys.*, 2009, **105**, 07E101.

3 C. Wäckerlin, K. Tarafder, D. Siewert, J. Girovsky, T. Hählen, C. Iacovita, A. Kleibert, F. Nolting, T. A. Jung, P. M. Oppeneer and N. Ballav, *Chem. Sci.*, 2012, **3**, 3154–3160.

4 C. Piamonteze, U. Flechsig, S. Rusponi, J. Dreiser, J. Heidler, M. Schmidt, R. Wetter, M. Calvi, T. Schmidt, H. Pruchova, J. Krempasky, C. Quitmann, H. Brune and F. Nolting, *J. Synchrotron Radiat.*, 2012, **19**, 661–674.

5 A. Uldry, F. Vernay and B. Delley, *Phys. Rev. B*, 2012, **85**, 125133.

6 C. Piamonteze, P. Miedema and F. M. F. de Groot, *Phys. Rev. B*, 2009, **80**, 184410.

7 Y. Teramura, A. Tanaka and T. Jo, *J. Phys. Soc. Jpn.*, 1996, **65**, 1053–1055.

8 B. Thole, P. Carra, F. Sette and G. van der Laan, *Phys. Rev. Lett.*, 1992, **68**, 1943–1946.

9 P. Carra, B. Thole, M. Altarelli and X. Wang, *Phys. Rev. Lett.*, 1993, **70**, 694–697.

10 T. Santos, J. Moodera, K. Raman, E. Negusse, J. Holroyd, J. Dvorak, M. Liberati, Y. Idzerda and E. Arenholz, *Phys. Rev. Lett.*, 2008, **101**, 147201.

11 C. Kittel, *Introduction to solid state physics*, Wiley, New York, 7th ed., 1996.

12 M. Bernien, X. Xu, J. Miguel, M. Piantek, P. Eckhold, J. Luo, J. Kurde, W. Kuch, K. Baberschke, H. Wende and P. Srivastava, *Phys. Rev. B*, 2007, **76**, 214406.

13 M. Bernien, J. Miguel, C. Weis, M. E. Ali, J. Kurde, B. Krumme, P. M. Panchmatia, B. Sanyal, M. Piantek, P. Srivastava, K. Baberschke, P. M. Oppeneer, O. Eriksson, W. Kuch and H. Wende, *Phys. Rev. Lett.*, 2009, **102**, 047202.